# Wavefront Velocity Oscillations of Carbon-Nanotube-Guided Thermopower Waves: Nanoscale Alternating Current Sources

**Joel T. Abrahamson,[†] Wonjoon Choi,[†,‡] Nicole S. Schonenbach,[†] Jungsik Park,[†] Jae-Hee Han,[†] Michael P. Walsh,[†] Kourosh Kalantar-zadeh,[†,§] and Michael S. Strano[†,*]**

[†]Department of Chemical Engineering and [‡]Department of Mechanical Engineering, Massachusetts Institute of Technology, Cambridge, Massachusetts 02139, United States and [§]School of Electrical and Computer Engineering, RMIT University, Melbourne, VIC, Australia

**ABSTRACT** The nonlinear coupling between exothermic chemical reactions and a nanowire or nanotube with large axial heat conduction results in a self-propagating thermal wave guided along the nanoconduit. The resulting reaction wave induces a concomitant thermopower wave of high power density (>7 kW/kg), resulting in an electrical current along the same direction. We develop the theory of such waves and analyze them experimentally, showing that for certain values of the chemical reaction kinetics and thermal parameters, oscillating wavefront velocities are possible. We demonstrate such oscillations experimentally using a cyclotrimethylene-trinitramine/multiwalled carbon nanotube system, which produces frequencies in the range of 400 to 5000 Hz. The propagation velocity oscillations and the frequency dispersion are well-described by Fourier's law with an Arrhenius source term accounting for reaction and a linear heat exchange with the nanotube scaffold. The frequencies are in agreement with oscillations in the voltage generated by the reaction. These thermopower oscillations may enable new types of nanoscale power and signal processing sources.

**KEYWORDS:** carbon nanotubes · cyclotrimethylene-trinitramine · thermopower · power source · oscillation · reaction diffusion · energy storage

There is a growing interest in the development of micro- or nanosized energy storage[1,2] and harvesting systems[3−9] that are capable of releasing energy at high rates. This is motivated by emerging applications such as so-called "smart dust",[10] microelectromechanical systems,[11] disposable medical diagnostics,[12,13] and flexible electronic devices.[14] However, power sources capable of the direct conversion of chemical energy to oscillating current do not exist, despite obvious applications of alternating current waveforms such as cardiac defibrillation and pacemaker signals,[12,15] micropiezoelectric oscillators,[4] RF identification tags,[16] and micromixers.[17] In this work, we investigate the nonlinear coupling between exothermic chemical reactions and a nanotube or nanowire with large axial heat conduction, resulting in self-propagating thermal waves guided along the nanoconduit. The resulting reaction wave induces a concomitant thermopower wave of high power density (>7 kW/kg), resulting in an electrical current that travels along the same direction. We show that such waves are predicted to demonstrate oscillatory front velocities under certain values of the chemical reaction rate constants and thermal parameters. These oscillations are verified experimentally using a cyclotrimethylene-trinitramine (TNA)/multiwalled carbon nanotube (MWNT) system and find a dominant frequency at approximately 430 Hz. We show that the oscillations and the frequency dispersion are well-described using a diffusive heat transfer model with a nonlinear source term coupled to a reactive mass balance along the nanoconduit.

Carbon nanotubes (CNTs) have several advantages for propagating these thermopower waves, despite possessing unexceptional Seebeck coefficients (approximately 80 μV/K).[18] They remain stable during high-temperature anaerobic reactions, and their axial thermal conductivity is exceedingly high,[19] resulting in large reaction front velocities and therefore large specific power outputs. The surface-to-volume ratios are also large for ordered 2D and 3D arrays of nanotubes, resulting in sizable heat exchange rates. Conversely, high Seebeck coefficient materials such as $Bi_2Te_3$ and $Sb_2Te_3$ are counterintuitively not favorable for guiding thermopower waves due to their low thermal conductivities.

In this work, we use cyclotrimethylene-trinitramine (TNA) as the fuel source due to its large enthalpy of reaction and strong adhesion to CNTs. CNTs are wrapped in TNA,

*Address correspondence to strano@mit.edu.

Received for review July 12, 2010 and accepted December 10, 2010.

**Published online December 23, 2010.** 10.1021/nn101618y

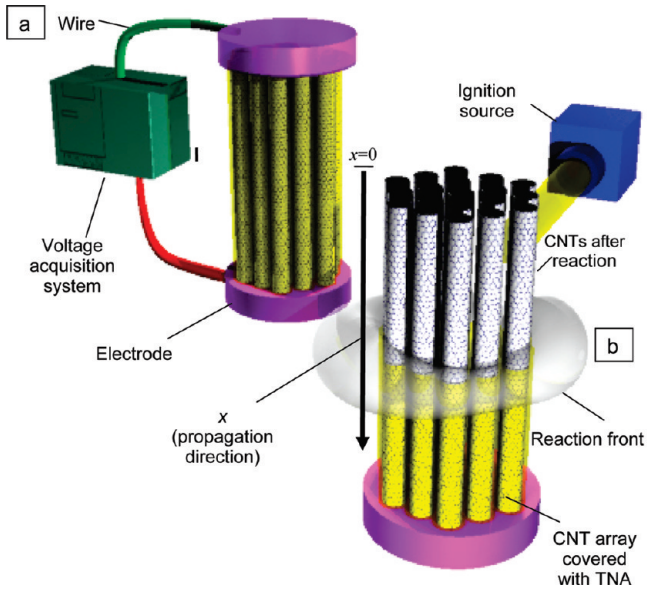


**Figure 1. (a) Schematic of the thermopower wave generator. (b) Ignition at one end of a cyclotrimethylene-trinitramine/multiwalled carbon nanotube (TNA−CNT) array results in an exothermic decomposition reaction that propagates along the CNT *via* its high axial thermal conductivity. The resulting thermal wave develops a concomitant thermopower wave of high power density.**

as shown in Figure 1; the reaction occurs at one end of this TNA−CNT system and propagates with the help of CNT conduits. We have previously demonstrated large power densities using TNA−CNT systems.[20] In this work, we show that the theory of such self-propagating thermal waves predicts distinct regimes where oscillatory wavefront velocities are possible and demonstrate their existence experimentally. Both theory and measurements are in agreement, with oscillations ranging in frequency from 400 to 5000 Hz.

**Theory of Thermopower Wave Oscillations.** We consider an annulus of material capable of first-order, exothermic decomposition (such as TNA) surrounding a carbon nanotube. Initiation of the chemical decomposition releases heat that travels much faster along the nanotube than in the annulus, resulting in a reaction wave guided by the CNT. We consider the diffusive transport limit where the reaction zone length exceeds that of the phonon mean free path in the CNT. The coupled thermal diffusion and chemical reaction terms can then be described using a modified Fourier's Law equation with a nonlinear source term to account for the chemical reaction. Under adiabatic conditions, the equation for the temperature of the annulus ($T$) becomes

$$\frac{\rho C_p}{M_W}\frac{\partial T}{\partial t} = \chi\frac{\partial^2 T}{\partial x^2} - (Qk_0 y)e^{(-E_a/RT)} - G_0\frac{4d_N}{d_M^2 - d_N^2}(T - T_2) \quad (1)$$

where $G_0$ is the interfacial conductance between the CNT and TNA, $d_M$ is the outer diameter of the TNA−CNT system, and $d_N$ is the CNT diameter. The parameter $\chi$ is the thermal conductivity, $\rho$ is the density, $Q$ is the enthalpy of reaction, $y$ is the molar concentration of reactive material, $k_0$ is the Arrhenius prefactor, $R$ is the universal gas constant, $E_a$ is the activation energy of decomposition, and $C_p$ and $M_W$ are the (molar) specific heat and molecular weight of the material, respectively. The second term on the right side accounts for the thermal source of the decomposition reaction, with the mole fraction of unreacted material ($y/y_0$) decreasing in time and space (according to the spatial profile of $T$) according to

$$\frac{\partial y}{\partial t} = -(k_0 y)e^{(-E_a/RT)} \quad (2)$$

The corresponding equation for the temperature ($T_2$) evolution in the carbon nanotube includes only terms for the heat transfer from the annulus and thermal diffusion:

$$\frac{\rho_2 C_{p,2}}{M_{W2}}\frac{\partial T_2}{\partial t} = \chi_2\frac{\partial^2 T_2}{\partial x^2} + G_0\frac{4}{d_N}(T - T_2) \quad (3)$$

where the subscript "2" refers to properties of the CNT. Equations 1 through 3 are solved using the following boundary conditions.

$$T_1(x, t = 0) = g \times e^{-x^2/w} + T_{ambient}$$

$$T_2(x, t = 0) = g \times e^{-x^2/w} + T_{ambient}$$

$$\frac{y}{y_0}(x > 0, t = 0) = 1$$

$$\frac{y}{y_0}(x = 0, t) =$$

0.001 (to approximate a zero boundary condition)

with the pulse width parameter $w = 2 \times 10^{-11}$ m$^2 \cdot \beta$. $T_{ambient}$ is the temperature of the surroundings, assumed to be 298 K. The parameter grouping $\beta = (C_p E_a)/(-QR)$ is the inverse dimensionless adiabatic reaction temperature rise, which is shown to be important for determining wave characteristics. The function $T(x, t = 0)$ is a Gaussian pulse, offset by 298 K, to simulate initiation by a rapid pulse of heat, for example, from a laser or resistive filament. Here, $g$ is the maximum initial temperature. From numerous simulations, we determined empirically that it must be greater than $0.16 \times \exp(0.37\beta)$ to initiate a propagating reaction wave. Physically, the magnitude of the temperature initial condition must increase with $\beta$ since that parameter is proportional to specific heat and activation energy. More energy must be supplied in the initial pulse for larger values of $\beta$ to overcome specific heat and activation energy and increase the initial reaction rate sufficiently to sustain self-propagation. The initial condition for the composition of the material, $y/y_0$, corresponds to a completely unreacted annulus, with the exception of the $x = 0$ boundary, which is almost entirely reacted so as to be consistent with the temperature condition, as

is necessary for numerical stability. The boundaries of the system are assumed to be adiabatic, and the system is made to be sufficiently long such that the wave is far from the boundaries. Further details of the simulation are given in the Methods section and in Supporting Information.

Our work is the first to examine this mathematical system of two coupled heat transport equations in conjunction with a chemical reaction. We have studied variants of these equations previously for the case of nanotube-guided nanothermites.[21] We also note that simplified versions of eqs 1 and 2 have been studied historically to describe 1D combustion waves and combustion synthesis.[22−25] Following Zel'dovich and Frank-Kamenetskii,[26] we nondimensionalize the system of equations. A nondimensional temperature $u = (R/E_a)T$, time $\tau = (-Qk_0R)/(C_pE_a)t$, and space $\xi = x((\rho C_p/\chi M_W)(-Qk_0R/C_pE_a))^{1/2}$ are shown to appropriately scale the system and resulting reaction wave.[23] A conversion $\eta$ can be defined $(M_W y)/\rho = 1 - \eta$. Other parameters of importance are the thermal diffusivities $\alpha = (\chi M_W/\rho C_p)$ of the annulus and of the nanotube, $\alpha_2$. The resulting equations are

$$\frac{\partial u}{\partial \tau} = \frac{\partial^2 u}{\partial \xi^2} + (1 - \eta)e^{-1/u} - \gamma_1(u - u_2) \quad (4)$$

$$\frac{\partial u_2}{\partial \tau} = \alpha_0 \frac{\partial^2 u_2}{\partial \xi^2} + \gamma_2(u - u_2) \quad (5)$$

$$\frac{\partial \eta}{\partial \tau} = \beta(1 - \eta)e^{-1/u} \quad (6)$$

where $\alpha_0 = \alpha_2/\alpha$, $\gamma_1 = (4d_N/d_M{}^2 - d_N^2)(G_0\beta M_W/\rho C_p k_0)$ and $\gamma_2 = (4G_0\beta M_{W2})/(d_N\rho_2 C_{p,2}k_0)$. Interestingly, this shows that the only terms affected by the diameter of the thermal conduit or the fuel layer are the interfacial heat exchange terms, $\gamma_1$ and $\gamma_2$. We have demonstrated with previous modeling work[20,21] that $\gamma_1$ and $\gamma_2$ do not affect the propagation of the reaction wave for values above $10^{-3}$; axial thermal transport within the nanotube becomes the limiting factor compared to interfacial conductance. By comparison, the simulations in this article used values on the order of $10^3$, so diameters have little effect to first order. A central motivation for this work is the fact that oscillatory behavior has been observed in similarly driven Fourier conduction systems;[23,27−30] hence, we ask if thermopower waves can likewise demonstrate regions of parameter space where oscillations are possible.

For $\beta$, $\alpha$, and $\alpha_2$, average values over the temperature range of 300 to 1700 K were used. Since $\beta$ is the nondimensionalized adiabatic reaction temperature rise, the maximum temperature was iterated until a consistent average $\beta$ of 10.6 for TNA was reached. Over the same range, $\alpha$ is $4.3 \times 10^{-8}$ m$^2$/s and $\alpha_2$ is 0.001 m$^2$/s. Depending on the concentration of defects, the thermal diffusivity of the nanotube, $\alpha_2$, may at least vary

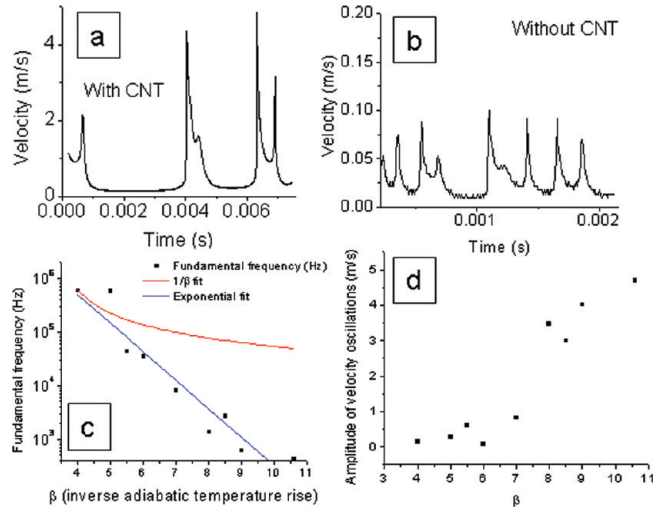


**Figure 2. (a) Simulation of the wavefront velocity using $\beta = 10.6$, $\alpha = 4.3 \times 10^{-8}$ m$^2$/s, and $\alpha_2 = 0.001$ m$^2$/s, with a length of 5 mm. The diameter of the nanotube was 22 nm, and the surrounding fuel annulus was 7 nm thick. (b) Simulated velocity for the same parameters with no nanotube ($\alpha_2 = 0$). (c) Fundamental frequency variation with $\beta$. The relation is inverse and stronger than simple dimensional scaling ($1/\beta$) would suggest. (d) Amplitude of oscillations for different $\beta$ values. Amplitudes are small and relatively constant for $\beta < 7$.**

over an order of magnitude. The value chosen here was the median. For all other parameters except $k_0$, the same values were used as in previous studies.[20]

The parameter $k_0$ affects the scaling of both the reaction wavefront velocity (henceforth referred to as velocity) and oscillation frequencies when they are converted from the nondimensional solutions of eqs 4−6 through the space and time scaling factors. The velocity and frequency depend on $k_0{}^{1/2}$ and $k_0$, respectively. Since $k_0$ is an *effective* Arrhenius constant, it can include mass and thermal diffusion limitations. We argue that the presence of the nanoconduit may reduce $k_0$ for the reacting material, TNA. While the MWNTs act as thermal conduits, kinetically they are inert, so their effect on $k_0$ may be more similar to that of a binder. Oyumi[31] measured $k_0$ in pure TNA to be $3.75 \times 10^{18}$ s$^{-1}$, whereas Williams and Matei[32] found it to be $2.0 \times 10^{11}$ s$^{-1}$ in a TNA/binder mixture over the range of 180 to 225 °C. Consequently, in order to reproduce the reaction wave velocity in the range of 0.1 to 2 m/s, which was in agreement with the experiments, $k_0 = 3 \times 10^9$ s$^{-1}$ was chosen. The validity of the choice was further confirmed by the excellent agreement between the simulation and measurements signature frequencies, which will be described later.

We first note that the simulations predict velocity oscillations for the TNA−CNT system. Figure 2a shows the velocity profile, beginning at $t = 0.2$ ms in order to see the steady-state responses after the initial period, which is more strongly influenced by the initial condition. Velocity is calculated by tracking the position of the point on the reaction temperature profile where nondimensional temperature is $1/(2\beta)$, which corresponds to 700

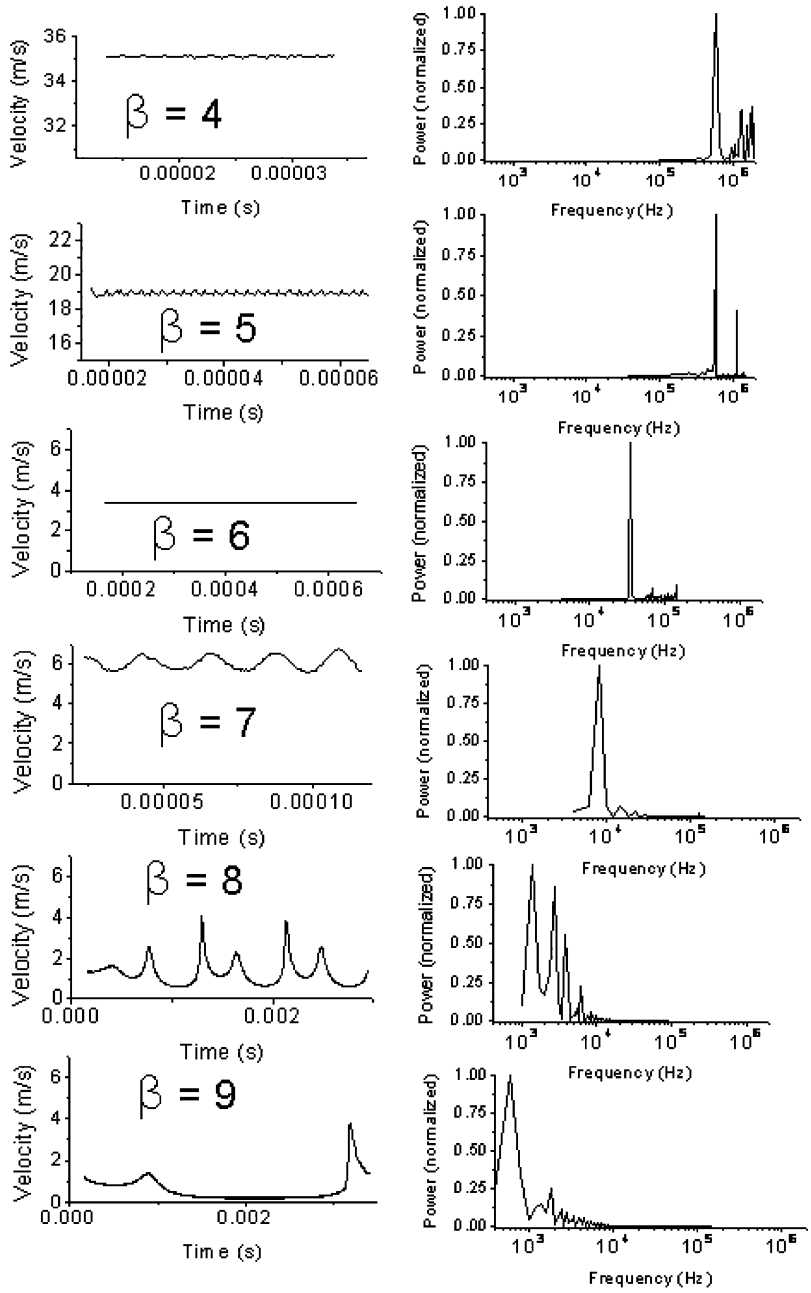


**Figure 3. Wavefront velocity profiles and frequency spectra for $4 < \beta < 9$. As β increases, so does the amplitude of the oscillations, and for $\beta > 7$, they begin to take on additional structure and complexity. Stronger secondary peaks in the frequency spectra arise at the same point.**

K. The average velocity is 0.56 m/s, although the amplitude of the oscillations is as large as 4.7 m/s. The oscillations are not simply sinusoidal but rather exhibit multiple components at different phase shifts. The mode velocity measured in our previous thermopower experiments was approximately 0.2 m/s,[20] so the simulation agrees reasonably well with our measurements. The overprediction is likely due to the adiabatic conditions of the simulation, particularly the exclusion of radiation, which will be further explored in future work.

Including a nanoscale thermal conduit increases the average velocity. The simulated velocity for TNA reacting without CNT thermal conduits is shown in Figure 2b. With no conduit, velocity is on average 0.031 m/s, and the amplitude of oscillations is 0.088 m/s. Including a nanoconduit of $\alpha_2 = 0.001$ m$^2$/s increases the average velocity by a factor of 18 and amplitude by a factor of 53. The rapid thermal transport in the thermal conduits affects the wavefront nonlinearly; they accelerate the reaction wave more when it is moving quickly than when it is moving slowly.

The presence of CNT thermal conduits also decreases the fundamental frequency, as measured using Fourier transforms (FTs) of the velocity profiles. We note that our simulation predicts frequencies on the order of kilohertz. For $\beta = 10.6$, the fundamental frequency

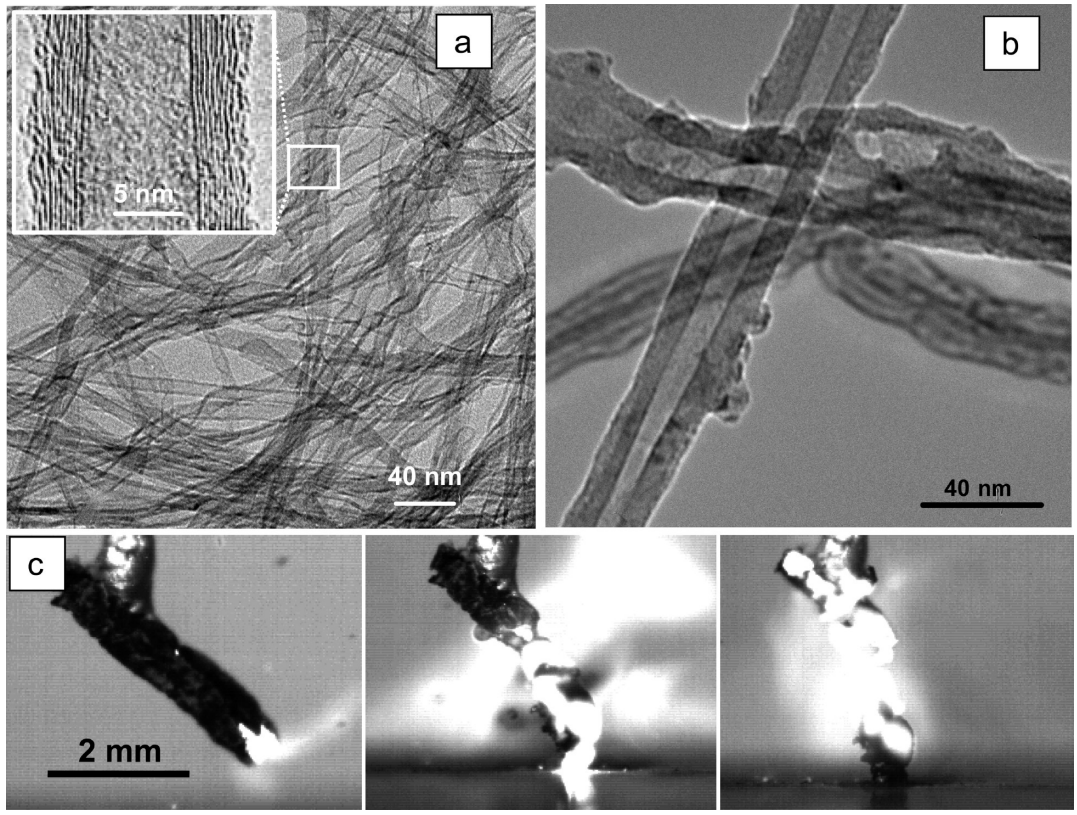


**Figure 4. (a) TEM images of MWNTs and (b) TNA−MWNTs after dispersion. (c, left to right) Reaction front photos using a high-speed camera. The length of the TNA−MWNTs is ~3 mm.**

decreases from 2350 to 420 Hz after the addition of a thermal conduit, compared to the case without one (Figure 2a,b). This is proportionately smaller than the increase in velocity. It could be that the non-uniform velocity acceleration from the conduits depletes the total energy of the reacting system such that it then takes more time for energy to build up to enable another rapid propagation phase. Future work will develop comprehensive steady-state and transient reactive wave theories that will expand upon these results, but such developments are outside of the scope of this work.

The frequency of these velocity oscillations is inversely related to β, but the dependence is stronger than 1/β, which is what would be expected if it were only due to the time dimensional scaling, $t = (\beta/k_0)\tau$. Figure 2c shows the fundamental frequencies for different β values. As with many properties of the reaction wave, including velocity (see Supporting Information), the relation to β appears to be an inverse exponential of the form $Ae^{-Z\beta}$, where $A$ is $6.9 \times 10^7$ Hz and $Z$ is 1.23 for the best fit to the simulation results. These simulation results indicate that we may be able to control oscillation frequencies in actual devices by using fuels with different properties, corresponding to different β values.

The amplitude of oscillations also depends on β, but not inversely, as frequency and average velocity do, as can be seen in Figure 2d. For $\beta < 7$, velocity oscillations are so small as to be inconsequential (although they have well-defined frequencies). Above that point, the relationship is approximately linear; velocity oscillation amplitude increases even as the average velocity is decreasing. This is consistent with the idea that CNT thermal conduits accelerate the reaction wave more when it is moving faster.

The value of β defines two distinct propagation regimes related to oscillations. Figure 3 shows velocity profiles and frequency spectra for $4 < \beta < 9$ at a constant value of $\alpha_2 = 0.001$ m$^2$/s. Although the average steady-state velocity decreases roughly exponentially from 35 to 0.56 m/s as β increases from 4 to 10.6, the change in oscillations is more complex and transitions from very low amplitude, almost constant velocity profiles to significant oscillations, often with multiple frequency components. This transition occurs between $\beta = 6$ and $\beta = 7$ and is also marked by the appearance of stronger secondary peaks and harmonics in the frequency spectra. Furthermore, we observe a local minimum in average velocity at $\beta = 6$, which coincides with the transition between propagation regimes. For $\beta > 8$, the velocity oscillations are interspersed with regions of very low, nearly constant velocity.

**Experimental Observations of Thermopower Wave Oscillations.** Vertically aligned multiwalled carbon nanotubes (MWNTs) served as the thermal conduits for our thermopower wave experiments. Figure 4a shows transmission electron micrographs (TEM) of the MWNTs after

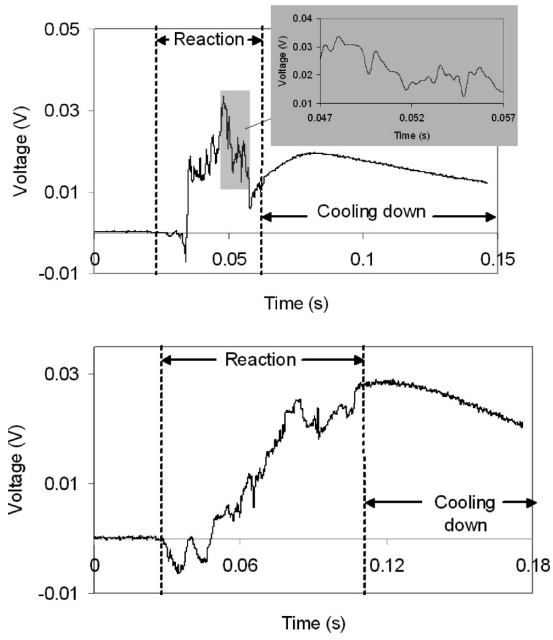


**Figure 5. Thermopower voltage signals in reaction (oscillation) and cooling zones. Voltage graphs for (top) a small (0.2 mg) and (bottom) a large mass (3 mg) sample of TNA−MWNTs.**

dispersion. They have, on average, an outer diameter of 22 nm, an inner diameter of 14 nm, and 10 walls. The arrays of these MWNTs were 3−5 mm tall with porosity of approximately 99% prior to the addition of TNA. Figure 4b shows the MWNTs after they have been coated with TNA; the continuous annuli are on average 7 nm thick and do not disrupt the MWNTs structurally. After evaporation, the porosity of the arrays was about 90%. Reaction and thermal waves propagated rapidly along the aligned MWNT arrays, as depicted in Figure 4c. Further experimental details can be found in the Methods section.

The accelerated reaction wave drives a concomitant wave of electrons, which also exhibits oscillations in voltage. As an example, Figure 5 shows voltages measured with an oscilloscope across two samples of different masses (0.2 and 3 mg). Large temperature gradients generate voltages with peak magnitudes in the range of 20 to 150 mV. Oscillations modulated this voltage with amplitudes in the range of 2 to 20 mV.

The voltage profiles in Figure 5 can be divided into two phases: a strong initial reaction phase (oscillation/noise) and a cooling (smooth) phase. Comparison between high-speed video and the electrical signals shows that the oscillation region corresponds to the time the reaction waves are propagating. The shape of the voltage profiles appears to depend on the sample mass: the larger the mass, the longer the oscillation phase. The longer voltage rise time in larger mass samples can be ascribed to slower reaction orthogonal to the MWNTs compared to axial propagation. Despite their very large axial thermal conductivity,[33] MWNT arrays' radial thermal conductivities are very low. In a TNA−MWNT system with TNA layers only a few nanometers thick and nanotube wall spacing of less than 1 nm, as well as large voids between nanotubes, phonon scattering in radial directions is substantial.[34] The maximum specific power exceeded 7 kW/kg for smaller mass samples, which is substantially larger than that of high-performance Li-ion batteries.

In agreement with our simulations, the voltage oscillations measured are likewise in the frequency range of 0−5000 Hz. The Fourier transforms of voltage signals from the oscillating reaction phases of four different samples of different masses are shown in Figure 6a. Approximately 40% of all samples had similar frequency signatures, whereas the remainder did not exhibit that pattern. The broad peak around zero frequency extends out to 330 Hz. In addition, there are distinct oscillation peaks at 430, 700, 960, 1230, 1490, ... and 4960 Hz. Except for the first two peaks, the peaks are equally spaced by ~260 Hz. These samples came from three different MWNT arrays, had varying cross-sectional areas and masses, and their densities varied up to 20%. However, interestingly, they all show similar frequency signatures. Since the same CVD process produced all samples, the MWNT diameter is consistent between samples (as confirmed by TEM), and thus the (per nanotube) thermal diffusivity is similar between samples.

As can be seen in Figure 6b, the FT of the graph of simulated velocity (Figure 2a) has frequency peaks at very similar positions. Some of these peaks are harmonics that have been broadened and shifted due to noise or finite sampling time, but the velocity oscillations also have multiple fundamentals. The peaks appear at 420, 970, 1250, 1530, ... and 4590 Hz, intervals of ~300 Hz, although not all peaks experimentally observed appear in the simulation.

The parity plot in Figure 6c demonstrates the agreement between the frequencies of the calculated velocity oscillations at $\beta = 10.6$ and the frequencies observed in the experimental voltage oscillations. A simple pairing of fundamental peaks and higher harmonics yields less than a 4% error between the simulated and experimental frequencies, corresponding to the "matching harmonics" data set. There appear to be peaks in the experimental FTs that are not reproduced in the simulated frequencies, for example, at 700, 1750, and 2540 Hz. If one instead assumes that *all* peaks experimentally observed constitute the harmonics, the error is larger at 20−40%, corresponding to the "no interpolated peaks" data set. There is sufficient evidence to support the former analysis (*i.e.*, matching up harmonics). A careful examination of the FT in Figure 6b shows that the 700 Hz harmonic forms the "shoulder" of the 420 Hz peak, and the magnitude of higher frequency harmonics may not be intense enough to detect above the spectrum background. Note that the points in the parity plot are parametric in the numerical order of each peak. With either comparison, however, it is clear that

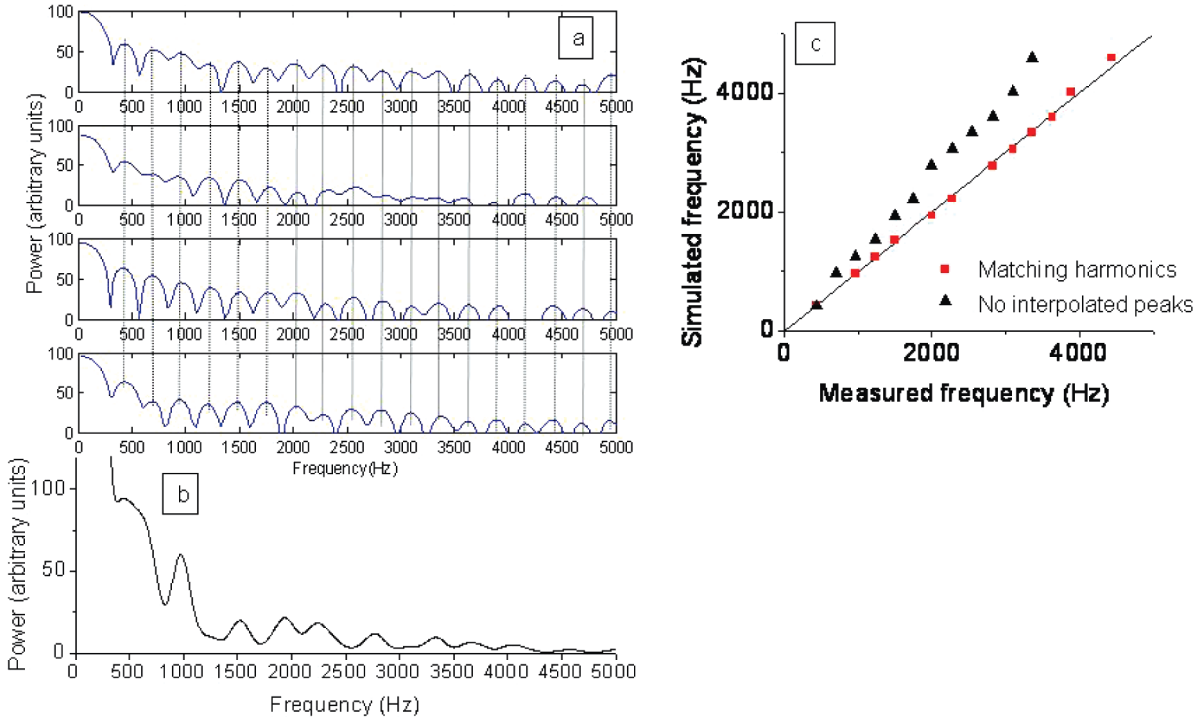


**Figure 6. (a) Frequency signatures of reaction region of voltage signals of four samples with different masses (top to bottom: 0.2, 0.9, 1.5, and 3 mg). The dotted lines show the signatures' agreement. Distinct frequency peaks are observed at 430, 700, 960, ... and 4960 Hz. (b) Fourier transform of the simulated velocity. Frequency peaks appear at 420, 970, 1250, ... and 4590 Hz. (c) Parity plot showing agreement between frequency peaks from velocity simulations and voltage measurements. The parameter changing between points is the number of the frequency peak. The agreement improves by matching the harmonics in the two spectra.**

there are discretized frequencies predicted by the Fourier analysis and observed experimentally. This supports the accuracy of the mathematical model, which predicts both average velocity (Figure 2a), 0.56 m/s, as well as the frequency of oscillations. Average velocities measured in thermopower experiments ranged from 0.05 to 1.35 m/s, and a range of values of $\beta$ and $\alpha_2$ could reproduce these.[20] It is notable, therefore, that the results of simulations using $\beta = 10.6$, $\alpha_2 = 0.001$ m$^2$/s, and $k_0 = 3 \times 10^9$ s$^{-1}$ agreed well with measurements of velocity, as well as with the frequency spectrum of voltage oscillations.

The parity between the frequencies of the velocity oscillations and the induced voltage implies that the wave velocity is the dominant factor in driving the current along the device. In the limit of conventional, steady-state thermopower (where wave velocity has no influence), the produced voltage, $V$, is based on the temperature difference alone:

$$V = \kappa(T_{rxn} - T_{ambient}) \quad (7)$$

Here $\kappa$ is the Seebeck coefficient and $T_{rxn}$ is the reaction temperature. Note that this expression possesses a Fourier transform that necessarily integrates to zero because $T_{rxn}$ is approximately constant. The fact that $V$ instead has a nonzero Fourier transform, related to the oscillations of the physical wavefront, supports the existence of a velocity component to the generated thermopower. This concept of a velocity component is consistent with our previous observations that samples producing larger velocity (evident in smaller mass samples, for example) generate higher specific power. The origin of the velocity component is currently under investigation, but one physical picture that is suggestive is that of a carrier entrainment that accompanies the wave propagation. Electron−phonon coupling in nanoscale systems is known to be enhanced, with carbon nanotubes being no exception.[35] One can calculate an order-of-magnitude estimate of such an entrainment current, $J$:

$$J = \frac{V}{R_e} = n \times A \times v \times e \quad (8)$$

where $R_e$ is the resistance of the bundle, $n$ is the carrier density of one CNT, $A$ is the cross-sectional area of the bundle, and $e$ is the elementary charge, and $v$ remains the thermopower wave velocity. For a typical current observed from systems experimentally tested to date (0.1−1 mA), we calculate a linear carrier density, $nA$, of 0.6 to 6 $\times$ 10$^{16}$ carriers/m or 0.6 to 6 carriers per nanometer of nanotube since there are about 10$^7$ nanotubes per sample. Given the size of a typical CNT unit cell (<1 nm), this estimate is reasonable.

In summary, we have both experimentally and theoretically investigated the behavior of the thermopower wave microgenerator. MWNT conduits axially accelerate the highly exothermic decomposition of TNA, generating voltage and current. The maximum DC specific

power of the thermopower wave system exceeds 7 kW/kg, which is larger than any generated by current Li-ion batteries. The system also shows strong auto-oscillatory behavior, described by chemical reaction and heat transfer equations and suitable boundary conditions, and these equations can accurately reproduce measured frequency signatures in the range of 0.4 to 5 kHz. This system represents a new class of microscale power sources for applications in which very large power densities are required, within limited space.

## METHODS

As with our previous simulations,[20] we solved eqs 1, 2, and 3 using the COMSOL Multiphysics software package with adaptive time steps and at various spatial mesh sizes (8−250 nm) over lengths of 2−5 mm to check for convergence. The diameter of the nanotube was 22 nm, and the surrounding fuel annulus was 7 nm thick, matching the physical system used in this work. The amplitude of the initial pulse could be varied by at least 50% without affecting the solution when a nanotube was present. As examples, the dimensional forms of two initial temperature conditions are calculated here. For $\beta = 4$, $g = 11\,000$ K and $w = 8 \times 10^{-11}$ m$^2$. For $\beta = 10.6$, $g = 124\,000$ K and $w = 2.1 \times 10^{-10}$ m$^2$. These pulses have a full width at half-maximum of 15 and 24 μm, respectively.

Previous modeling work demonstrated that interfacial heat transfer does not limit the wavefront propagation for $G_0 > 10^5$ W/m$^2$/K, corresponding to $\gamma_1$ and $\gamma_2 > 10^{-3}$ as described before.[20] The simulations were carried out for durations sufficient to observe steady waves with multiple periods of oscillation. A Matlab program extracted the temperature data and calculated velocity. Our previous modeling work has shown that convection does not significantly affect velocity in the TNA−CNT system, and that averaging property values such as thermal conductivity, enthalpy of reaction, and specific heat over an appropriate temperature range results in agreement with simulation using temperature-dependent parameters.[20]

For our experiments, we synthesized vertically aligned MWNTs using chemical vapor deposition in a horizontal quartz tube furnace with Fe and $Al_2O_3$ catalytic layers. Ethylene ($C_2H_4$), hydrogen ($H_2$), and argon (Ar) were used as the carbon source, catalytic, and carrier gases, respectively.[36] To coat the MWNT arrays, a quantity of 200 mg of TNA was dissolved in 10 mL of acetonitrile and filtered. This solution was dropped on the arrays and then evaporated under atmospheric conditions for several hours, coating the nanotubes. $NaN_3$ in aqueous solution (50 mg/mL) was then added to serve as a primary igniter to lower activation energy (40 kJ/mol for $NaN_3$, in contrast to 130−200 kJ/mol for TNA). Silver paste was used to make electrical connections between the TNA−MWNT samples and copper tape electrodes. Their resistance ranged from 10 to 100 Ω depending on the size of the TNA−MWNT bundle. Over 100 samples of different masses were prepared and tested as reported previously.[20]

The samples were ignited at one end of the bundles with a 400 mW laser of 785 nm wavelength. The propagation of the reaction front was measured optically using a high-speed CCD camera (CPL-MS70K, Canadian Photonic Laboratories) with a microscopic lens (Macro 60 mm, f/2.8D micro Nikkor Autofocus lens, Nikon) at up to 90 000 frames per second.

*Acknowledgment.* This work was supported by the Air Force Office of Scientific Research. The authors thank the Department of Innovation, Industry, Research and Science, Australia (ISL Grant No. CG130115) for financially supporting K.K.'s travel to MIT as a visiting scientist. J.T.A. and W.C. acknowledge fellowship support from the National Science Foundation and ILJU Foundation of Education and Culture, respectively.

*Supporting Information Available:* Further description and details of the numerical solution methods, as well as a summary of the relation between average velocity and β. This material is available free of charge *via* the Internet at http://pubs.acs.org.

## REFERENCES AND NOTES

1. van den Berg, A. W. C.; Arean, C. O. Materials for Hydrogen Storage: Current Research Trends and Perspectives. *Chem. Commun.* **2008**, 668–681.
2. Simon, P.; Gogotsi, Y. Materials for Electrochemical Capacitors. *Nat. Mater.* **2008**, *7*, 845–854.
3. Qin, Y.; Wang, X. D.; Wang, Z. L. Microfibre−Nanowire Hybrid Structure for Energy Scavenging. *Nature* **2008**, *451*, 809–813.
4. Song, J. H.; Zhou, J.; Wang, Z. L. Piezoelectric and Semiconducting Coupled Power Generating Process of a Single ZnO Belt/Wire: A Technology for Harvesting Electricity from the Environment. *Nano Lett.* **2006**, *6*, 1656–1662.
5. Mor, G. K.; Varghese, O. K.; Paulose, M.; Shankar, K.; Grimes, C. A. A Review on Highly Ordered, Vertically Oriented $TiO_2$Nanotube Arrays: Fabrication, Material Properties, and Solar Energy Applications. *Sol. Energy Mater. Sol. Cells* **2006**, *90*, 2011–2075.
6. Shao, Z. P.; Haile, S. M.; Ahn, J.; Ronney, P. D.; Zhan, Z. L.; Barnett, S. A. A Thermally Self-Sustained Micro Solid-Oxide Fuel-Cell Stack with High Power Density. *Nature* **2005**, *435*, 795–798.
7. Strasser, M.; Aigner, R.; Lauterbach, C.; Sturm, T. F.; Franosch, M.; Wachutka, G. Micromachined CMOS Thermoelectric Generators as On-Chip Power Supply. *Sens. Actuators, A* **2004**, *114*, 362–370.
8. Mitcheson, P. D.; Yeatman, E. M.; Rao, G. K.; Holmes, A. S.; Green, T. C. Energy Harvesting from Human and Machine Motion for Wireless Electronic Devices. *Proc. IEEE* **2008**, *96*, 1457–1486.
9. Arnold, D. P. Review of Microscale Magnetic Power Generation. *IEEE Trans. Magn.* **2007**, *43*, 3940–3951.
10. Cook, B. W.; Lanzisera, S.; Pister, K. S. J. SoC Issues for RF Smart Dust. *Proc. IEEE* **2006**, *94*, 1177–1196.
11. Cook-Chennault, K. A.; Thambi, N.; Sastry, A. M. Powering MEMS Portable Devices—A Review of Non-regenerative and Regenerative Power Supply Systems with Special Emphasis on Piezoelectric Energy Harvesting Systems. *Smart Mater. Struct.* **2008**, *17*, 043001.
12. Kerzenmacher, S.; Ducree, J.; Zengerle, R.; von Stetten, F. Energy Harvesting by Implantable Abiotically Catalyzed Glucose Fuel Cells. *J. Power Sources* **2008**, *182*, 1–17.
13. Yager, P.; Edwards, T.; Fu, E.; Helton, K.; Nelson, K.; Tam, M. R.; Weigl, B. H. Microfluidic Diagnostic Technologies for Global Public Health. *Nature* **2006**, *442*, 412–418.
14. Klauk, H.; Zschieschang, U.; Pflaum, J.; Halik, M. Ultralow-Power Organic Complementary Circuits. *Nature* **2007**, *445*, 745–748.
15. Zadeh, A. E. In *IEEE 2008 51st Midwest Symposium on Circuits and Systems*; IEEE: New York, 2008; Vols. *1* and *2*, pp 29−32.
16. Pillai, V.; Heinrich, H.; Dieska, D.; Nikitin, P. V.; Martinez, R.; Rao, K. V. S. An Ultra-low-Power Long Range Battery/Passive RFID Tag for UHF and Microwave Bands with a Current Consumption of 700 nA at 1.5 V. *IEEE Trans. Circuits Syst. I* **2007**, *54*, 1500–1512.
17. Ottino, J. M.; Wiggins, S. Introduction: Mixing in Microfluidics. *Philos. Trans. R. Soc. London, Ser. A* **2004**, *362*, 923–935.
18. Kim, P.; Shi, L.; Majumdar, A.; McEuen, P. L. Thermal Transport Measurements of Individual Multiwalled Nanotubes. *Phys. Rev. Lett.* **2001**, *8721*, 215502–215505.

19. Yu, C. H.; Shi, L.; Yao, Z.; Li, D. Y.; Majumdar, A. Thermal Conductance and Thermopower of an Individual Single-Wall Carbon Nanotube. *Nano Lett.* **2005**, *5*, 1842–1846.
20. Choi, W.; Hong, S.; Abrahamson, J. T.; Han, J.-H.; Song, C.; Nair, N.; Baik, S.; Strano, M. S. Chemically Driven Carbon Nanotube-Guided Thermopower Waves. *Nat. Mater.* **2010**, *9*, 423–429.
21. Abrahamson, J. T.; Nair, N.; Strano, M. S. Modelling the Increase in Anisotropic Reaction Rates in Metal Nanoparticle Oxidation Using Carbon Nanotubes as Thermal Conduits. *Nanotechnology* **2008**, *19*, 195701–195708.
22. Xin, J. Front Propagation in Heterogeneous Media. *SIAM Rev.* **2000**, *42*, 161–230.
23. Weber, R. O.; Mercer, G. N.; Sidhu, H. S.; Gray, B. F. Combustion Waves for Gases (Le=1) and Solids (L->Infinity) . *Proc. R. Soc. London, Ser. A* **1997**, *453*, 1105–1118.
24. Kolmogorov, A. N.; Petrovsky, I. G.; Piskunov, N. S. Etude de l'équation de la diffusion avec croissance de la quantité de matière et son application à un problème biologique. *Moskow Univ. Math. Bull.* **1937**, *1*, 1–25.
25. Fisher, R. A. The Wave of Advance of Advantageous Genes. *Ann. Eugenics* **1937**, *7*, 355–369.
26. Zel'dovich, Y. B.; Frank-Kamenetskii, D. A. The Theory of Thermal Flame Propagation. *Zh. Fiz. Khim.* **1938**, *12*, 100–105.
27. Zeldovich, Y. B.; Leypunsky, O. I.; Librovich, V. B. *Theory of Non-Steady Powder Combustion*; Izdak: Nauka Moscow, 1975.
28. Bayliss, A.; Matkowsky, B. J. From Traveling Waves to Chaos in Combustion. *SIAM J. Appl. Math.* **1994**, *54*, 147–174.
29. Shkadinskii, K. G.; Khaikin, B. I.; Merzhanov, A. G. Propagation of a Pulsating Exotermic Reaction Front in Condensed Phase. *Combust. Explos. Shock Waves* **1971**, *7*, 15–22.
30. Merzhanov, A. G.; Filonenko, A. K.; Borovinska, Y. A. New Phenomena in Combustion of Condensed Systems. *Dokl. Akad. Nauk SSSR* **1973**, *208*, 892–894.
31. Oyumi, Y. Melt Phase Decomposition of RDX and Two Nitrosamine Derivatives. *Propellants, Explosives, Pyrotechnics* **1988**, *13*, 42–47.
32. Williams, M. R.; Matei, M. V. The Decomposition of Some RDX and HMX Based Materials in the One-Dimensional Time to Explosion Apparatus. Part 1. Time to Explosion and Apparent Activation Energy. *Propellants Explosives Pyrotechnics* **2006**, *31*, 435–441.
33. Mingo, N.; Broido, D. A. Carbon Nanotube Ballistic Thermal Conductance and Its Limits. *Phys. Rev. Lett.* **2005**, *95*, 096105.
34. Chen, G. Thermal Conductivity and Ballistic-Phonon Transport in the Cross-Plane Direction of Superlattices. *Phys. Rev. B* **1998**, *57*, 14958–14973.
35. Pop, E.; Mann, D.; Cao, J.; Wang, Q.; Goodson, K.; Dai, H. J. Negative Differential Conductance and Hot Phonons in Suspended Nanotube Molecular Wires. *Phys. Rev. Lett.* **2005**, *95*, 155505–155508.
36. Xu, Y. Q.; Flor, E.; Schmidt, H.; Smalley, R. E.; Hauge, R. H. Effects of Atomic Hydrogen and Active Carbon Species in 1 mm Vertically Aligned Single-Walled Carbon Nanotube Growth. *Appl. Phys. Lett.* **2006**, *89*, 123116–123118.